Mean Flow Evolution of a Baroclinically Unstable Potential Vorticity Front

EMMANUEL BOSS AND LUANNE THOMPSON

School of Oceanography, University of Washington, Seattle, Washington

(Manuscript received 7 July 1997, in final form 5 March 1998)

ABSTRACT

Quasi-linear theory and numerical models are used to study the mean flow modification of a two-layer shallow water baroclinically unstable flow as a function of Rossby number. This flow has an upper-layer potential vorticity front overlying a quiescent lower layer and is used as a simple representation of the Gulf Stream.

Quantities derived from an analytical expansion in the small meander amplitude limit of the (quasi-linear) equations are found to compare quantitatively well with numerical model simulations of the flow in small amplitude and to pertain qualitatively even beyond the instability equilibration, where the meander amplitude is as large as the meander wavelength. The baroclinic evolution is similar for all Rossby numbers, with differences arising from increased asymmetry of the flow with increasing Rossby number. The equilibration of the instability is similar for all Rossby numbers and is due to the acceleration of a strong barotropic shear. This acceleration is predicted from the small amplitude analysis.

Quasigeostrophic diagnostics are shown to be useful even for large Rossby number flows such as the Gulf Stream. One qualitative difference that appears is that as the mean flow is modified, a lateral separation of the zonal mean potential vorticity front and the jet maximum appears, consistent with Gulf Stream observations. This feature is found only for finite Rossby number flows.

1. Introduction

Oceanic fronts, regions where changes in density and potential vorticity (PV) are observed over horizontal scales of the baroclinic deformation radius, are found in all of the world's oceans, at wind-driven gyre boundaries, in areas of coastal upwelling, in regions of Ekman convergence, and at river mouths. By geostrophy, PV and density fronts are associated with strong baroclinic jets.

The large available potential energy and kinetic energy stored in fronts often provide an energy source for growing instabilities. These instabilities cause meandering of the front and the formation of cyclones and anticyclones in the growing meanders. Consistent with linear stability theory, observations from the SYNOP study of the Gulf Stream (Watts et al. 1995; Shay et al. 1995) show that growing meanders in the Gulf Stream above the thermocline are always associated with cyclogenesis and strong velocities at depth ($\sim$0.4 m s^{-1} at 3500 m). Linear stability theory has been used to explain the growth rates and observed wavelengths of the meanders in the Gulf Stream (Killworth et al. 1984; Flierl and Robinson 1984). As one moves downstream in the Gulf Stream, the time-mean jet changes in response to the growing meanders. It is this feedback process that we study here.

Analysis of the effect of the growing instability on the initial flow structure can be most easily studied by constructing an initial flow with zonally periodic meanders. While not strictly applicable to oceanographic currents such as the Gulf Stream where the meanders grow in space (downstream of Cape Hatteras), the zonal-mean theory can provide insight into the Gulf Stream system by making the analogy between spatially growing meanders of the Gulf Stream and temporally growing meanders of zonally periodic models. In the context of such models, past studies of the interaction of mean flows and growing instabilities have been conducted in three distinct ways: 1) Weakly nonlinear analysis, which is an analytical approach that uses multiple timescale analysis that provides predictions for both small and large amplitude evolution but is limited to slightly supercritical flows (Pedlosky 1970). This method in many cases cannot be used to analyze the most unstable wave, the one most likely to be observed in geophysical flows. 2) Quasi-linear analysis (Phillips 1954), which is an analytical approach in which linearized forms of the governing equations are used by forming an amplitude expansion of the flow variables and can be used to analyze strongly supercritical flows but is limited to small amplitude meanders with normal mode wave structure. 3) Numerical analysis using fully nonlinear models

Corresponding author address: Dr. Emmanuel Boss, COAS, 104 Ocean Admin. Bldg., Oregon State University, Corvallis, OR 97331-5503.
E-mail: boss@oce.orst.edu

© 1999 American Meteorological Society

(e.g., Rhines 1977; Ikeda 1981; Wood 1988; Onken 1992). This method provides the evolution of any desired flow at all times. This analysis is, however, the least amenable to generalization (to other flows) since only a small subset of the flow parameter space can be explored and the dependences of the results on these parameters are not explicit in the numerical model.

In the present study the last two approaches, namely a quasi-linear analytical analysis and analysis of numerical model results, are employed to study the evolution of a baroclinically unstable PV front. The Rossby number of the flow is varied to allow comparison of the mean flow evolution of a quasigeostrophic (QG) front with that in a shallow water front with a large Rossby number. Our study is a natural extension of the studies of Phillips (1954) and Shepherd (1983), who analytically analyzed the small-amplitude quasi-linear mean flow modification equations of QG flows.

Quasigeostrophic theory has been used extensively in the examination and modeling of the Gulf Stream (Kim and Watts 1994; Ikeda 1981). We have shown in a previous paper (Boss et al. 1996, herein BPT) that in many ways QG linear theory does better than one would expect in the prediction of growth rates and wavelengths of most-unstable modes in the instability of a two-layer flow with a potential vorticity front in the upper layer. We use the same model here to study mean-flow evolution of a baroclinically unstable jet and show to what extent the conclusions that we made from the linear analysis apply to the quasi-linear and nonlinear situations and whether the quasi-linear predictions can be used to explain nonlinear evolution.

This paper is organized as follows: we introduce the PV-front model and derive the shallow water quasi-linear mean flow modification equations in section 2. The results of the quasi-linear approach are presented in section 3 where we compare them to numerical model results with small amplitude meanders. In section 4, the numerical model results with large amplitude meanders are presented. In sections 2 through 4 we concentrate on three particular flows: a flow with an $O(1)$ Rossby number, its QG limit, and an outcropping front with constant PV in the upper layer. In section 5 our results are summarized and contrasted with previous studies and Gulf Stream observations.

2. Formulation of the zonal mean equations

a. Governing equations and basic state

We construct a model that contains several essential elements for the study of a baroclinically unstable jet. A two-layer fluid with a meridionally confined zonal jet in the upper layer is considered. The Boussinesq, hydrostatic, rigid-lid, and f-plane approximations are applied. We refer this set of approximations as the shallow-water approximation (SW). For a two-layer SW flow, the momentum and continuity equations are

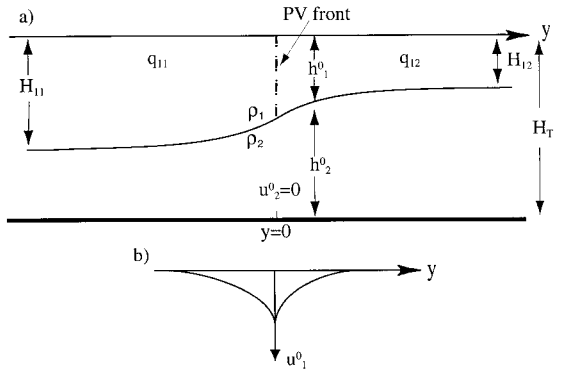

FIG. 1. Schematic of the depth (a) and velocity (b) fields of an upper-layer potential vorticity front. The upper-layer flow is geostrophic and has piecewise constant PV, $q_1^0 = q_{1j} = f/H_{1j}$, where j denotes the side of the front (1 being south, $y < 0$), H_{1j} denotes the depth of the upper layer at $y \to \mp\infty$, respectively, and the lower layer is quiescent. When $H_{12} = 0$, the interface between the layers intersects the surface, resulting in an outcropping front.

$$(\partial_t + \mathbf{u}_n \cdot \boldsymbol{\nabla})\mathbf{u}_n + f\mathbf{k} \times \mathbf{u}_n = -\boldsymbol{\nabla} p_n, \tag{1}$$

$$h_{nt} + \boldsymbol{\nabla} \cdot (h_n \mathbf{u}_n) = 0, \tag{2}$$

where the subscript $n = 1$ (2) denotes the upper (lower) layer, $\mathbf{u} = (u, v)$ is the horizontal velocity vector, f is the Coriolis parameter, $\boldsymbol{\nabla}$ is the horizontal differential operator, and $\mathbf{k}$ is the vertical unit vector. The layer's reduced pressure (p_n, the pressure divided by density) and depth (h_n) are related by the hydrostatic equation:

$$g'\boldsymbol{\nabla} h_1 = -g'\boldsymbol{\nabla} h_2 = \boldsymbol{\nabla}(p_1 - p_2), \tag{3}$$

where $g' \equiv g(\rho_2 - \rho_1)/\rho_1$ is the reduced gravity. Potential vorticity is conserved in each layer:

$$(\partial_t + \mathbf{u}_n \cdot \boldsymbol{\nabla}) q_n = 0, \qquad q_n \equiv \frac{f + \mathbf{k} \cdot \boldsymbol{\nabla} \times \mathbf{u}_n}{h_n}. \tag{4}$$

The basic flow whose nonlinear evolution is investigated here is a jet confined to the upper layer and trapped to the interface between two semi-infinite regions of constant PV. The potential vorticity is given by

$$q_1^0 = q_{1j} \equiv \frac{f}{H_{1j}},$$

where j denotes the side of this PV front (1 being south, $y < 0$), and H_{1j} the fluid depth at $y \to \mp\infty$ (Fig. 1). Requiring that the basic flow (denoted by superscript 0) be x independent, meridionally continuous in both layer depth and velocity, steady, geostrophic, and confined to the upper layer ($u_2^0 = 0$), the upper-layer depth is

$$h_1^0 = \begin{cases} H_{11}\left[\left(\left(\dfrac{H_{12}}{H_{11}}\right)^{1/2} - 1\right)\exp(y/R_{d,1}) + 1\right] & \text{for } y < 0 \\ H_{12}\left[\left(\left(\dfrac{H_{11}}{H_{12}}\right)^{1/2} - 1\right)\exp(-y/R_{d,2}) + 1\right] & \text{for } y > 0, \end{cases} \tag{5}$$

and the upper-layer velocity

$$u_1^0 = -\frac{g'}{f}\frac{dh_1}{dy} = U_0\begin{cases}\exp(y/R_{d,1}) & \text{for } y < 0\\ \exp(-y/R_{d,2}) & \text{for } y > 0,\end{cases} \quad (6)$$

where

$$U_0 = (g'H_{11})^{1/2} - (g'H_{12})^{1/2} \quad \text{and} \quad R_{d,j} \equiv (g'H_{1j})^{1/2}/f \quad (7)$$

are the jet maximum speed and the (different) deformation radii on each side of the front. The flow is confined to within a deformation radius of the potential vorticity front.

In order to study the mean flow modifications as a function of the Rossby number of the flow, it is convenient to nondimensionalize the equations by transforming

$$t \to \frac{tR_d}{U_0}, \qquad (x, y) \to (x, y)R_d, \qquad (u, v) \to (u, v)U_0,$$

$$h_i \to h_iH_1, \quad \text{and} \quad \psi_i \to p_i(g'H_1)^{1/2}U_0, \quad (8)$$

where

$$H_1 \equiv (H_{11} + H_{12})/2, \qquad R_d \equiv (g'H_1)^{1/2}/f, \quad (9)$$

and H_1 is the y-averaged upper-layer depth and R_d the radius of deformation based on H_1. The nondimensional Rossby number, $\epsilon \equiv |U_0|/fR_d$, is a measure of the strength and asymmetry of the initial geostrophic flow.

We define a scaled (by H_1) perturbation height,

$$\epsilon\eta_1 \equiv h_1 - 1, \qquad \epsilon\eta_2 \equiv h_2 - r + 1,$$
$$\text{that is,} \quad \eta_1 + \eta_2 = 0, \quad (10)$$

where $r \equiv H_T/H_1$ is the ratio of the total fluid depth to the mean upper-layer depth. The hydrostatic relation becomes

$$\nabla(\psi_1 - \psi_2) = \nabla\eta_1. \quad (11)$$

The resulting nondimensional governing equations [(1)–(2)] are

$$\epsilon(\partial_t + \mathbf{u}_n \cdot \nabla)\mathbf{u}_n + \mathbf{k} \times \mathbf{u}_n = -\nabla\psi_n, \quad (12)$$

$$\epsilon(\eta_{1,t} + \nabla \cdot (\eta_1\mathbf{u}_1)) + \nabla \cdot \mathbf{u}_1 = 0, \quad (13)$$

$$\epsilon(\eta_{2,t} + \nabla \cdot (\eta_2\mathbf{u}_2)) + (r - 1)\nabla \cdot \mathbf{u}_2 = 0, \quad (14)$$

and the nondimensional PV is given by

$$q_1 = \frac{1 + \epsilon\nabla \times \mathbf{u}_1}{1 + \epsilon\eta_1}, \qquad q_2 = \frac{1 + \epsilon\nabla \times \mathbf{u}_2}{r - 1 + \epsilon\eta_2}. \quad (15)$$

The nondimensional basic flow variables are calculated from (5)–(6):

$$u_1^0 = -\psi_{1y}^0 = \exp(-\alpha_j|y|),$$

$$\psi_1^0 = \text{sgn}(y)\left[\frac{1}{\alpha_j}(\exp(-\alpha_j|y|) - 1)\right], \qquad v_1^0 = 0,$$

$$v_2^0 = u_2^0 = \psi_2^0 = 0, \quad (16)$$

where $\alpha_j = R_d/R_{d,j}$. From the definitions of ϵ and α_j, Williams (1991) derived two relationships,

$$\epsilon = 1/\alpha_1 - 1/\alpha_2, \qquad (1/\alpha_1)^2 + (1/\alpha_2)^2 = 2, \quad (17)$$

which show that ϵ uniquely determines the mean flow in the upper layer. Together with r the basic state is specified. Without loss of generality, the north side ($y > 0$) is chosen to be shallower; $H_{11} > H_{12}$ (or $\alpha_2 > \alpha_1$); ϵ varies between zero and $\sqrt{2}$ while r varies from zero to infinity.

Special cases of the PV-front model used here were considered in the past and applied to the Gulf Stream, when $\epsilon = \sqrt{2}$, $H_{12} = 0$, and the model reduces to the outcropping front studied by Killworth et al. (1984). The QG case is recovered in the limit $\epsilon = 0$ (BPT). The above model in the limit $r \to \infty$ becomes the $1\frac{1}{2}$-layer model studied for $\epsilon = \sqrt{2}$ by Stommel (1965) and Paldor (1983), for variable ϵ by Williams (1991), and for $\epsilon = 0$ by Pratt and Stern (1986). In BPT and Boss (1996) we summarize the results found in those studies and interpret them in terms of the linearized waves found in them. In particular, we find that the PV-front model is baroclinically unstable for all values of ϵ and finite r and that the linearized QG solution approximates well the solutions found for all values of ϵ.

b. Zonal mean flow modification

To examine the modification to the zonal flow by the waves, the governing equations (12)–(14) are zonally averaged. Denoting the zonal average by an overbar and the deviation from it by a prime superscript,

$$\epsilon(\partial_t + \overline{\mathbf{u}}_n \cdot \nabla)\overline{\mathbf{u}}_n + \mathbf{k} \times \overline{\mathbf{u}}_n + \nabla\overline{\psi}_n = -\epsilon\overline{\mathbf{u}_n' \cdot \nabla\mathbf{u}_n'}, \quad (18)$$

$$\epsilon(\overline{\eta}_{1,t} + \nabla \cdot (\overline{\eta}_1\overline{\mathbf{u}}_1)) + \nabla \cdot \overline{\mathbf{u}}_1 = -\epsilon\overline{\nabla \cdot (\eta_1'\mathbf{u}_1')}, \quad (19)$$

$$\epsilon(\overline{\eta}_{2,t} + \nabla \cdot (\overline{\eta}_2\overline{\mathbf{u}}_2)) + (r - 1)\nabla \cdot \overline{\mathbf{u}}_2 = -\epsilon\overline{\nabla \cdot (\eta_2'\mathbf{u}_2')}. \quad (20)$$

The time rate of change of the zonal mean flow is forced by correlations of terms having no zonal mean structure (Phillips 1954). Equations (12)–(14) and (18)–(20) are applied in two different ways: first, we assume that the instability has small amplitude (and is thus early in its evolution) and expand the variables in the perturbation amplitude to find the quasi-linear equations describing the mean flow modifications. Then, the solutions of this analytical approach are compared with numerical so-

lutions of fully nonlinear and dissipative models by taking the results of the models and directly calculating (18)–(20).

c. Quasi-linear formulation

We use a perturbation method similar to that of Phillips (1954) and Shepherd (1983) to solve for the modification to the mean quantities using (12)–(14) and (18)–(20). We extend the work of Phillips (1954) and Shepherd (1983) by considering flow with finite Rossby number.

To understand the first-order effect of the unstable waves on the mean flow, the deviation from the basic-state flow is assumed to be small relative to the scales of the basic state [i.e., $\max(\theta') \ll 1$] and to have meridionally varying amplitudes and normal-mode structure,

$$\theta' = a\mathrm{Re}\{\theta'(y)e^{i(kx-\omega t)}\},$$

where θ denotes any variable and a denotes the initial amplitude of the perturbation. For unstable flows the frequency ω is complex with its imaginary part, ω_I, the growth rate. The solution for $\theta'(y)$ is found by linearizing (12)–(14) about the basic zonal-mean flow and solving for the normal modes (BPT).

The modification of the mean flow in the quasi-linear theory is then found by substituting the perturbation solution found by BPT into the rhs of (18)–(20). Since

$$\overline{\mathrm{Re}\{A(y)e^{i\phi}\}\mathrm{Re}\{B(y)e^{i\phi}\}} = \frac{1}{2}\mathrm{Re}\{A(y)B(y)^*\}e^{2\mathrm{Im}\{\phi\}},$$

where the asterisk denotes the complex conjugate and ϕ the phase, the mean flow modifications are $O(a^2)$ and are proportional to $e^{2\omega_I t}$. The mean flow variables are thus expanded in two orders in amplitude, $\overline{\theta} = \theta_0(y) + a^2\tilde{\theta}(y)e^{2\omega_I t}$.

Following the above prescription and keeping terms only to $O(a^2)$, the mean flow acceleration is given by

$$\epsilon\overline{u}_{nt}e^{-2\omega_I t} = 2\omega_I\epsilon\tilde{u}_n = -\tilde{v}_n(\epsilon u^0_{ny} - 1) - \epsilon\overline{v'_n u'_{ny}}, \quad (21)$$

$$\epsilon\overline{v}_{nt}e^{-2\omega_I t} = 2\omega_I\epsilon\tilde{v}_n = -\tilde{u}_n - \tilde{\psi}_{ny} - \epsilon\overline{u'_n v'_{nx}} - \epsilon\overline{v'_n v'_{ny}}. \quad (22)$$

Likewise, the zonal mean mass balance is

$$\epsilon\overline{\eta}_{nt}e^{-2\omega_I t} = 2\omega_I\epsilon\tilde{\eta}_{nt} = -(h^0_n\tilde{v}_n)_y - \epsilon(\overline{\eta'_n v'_n})_y. \quad (23)$$

Since there is no mean zonal pressure gradient, there cannot be a zonal-mean meridional geostrophic velocity. Thus $\tilde{v}_n$ is $O(\epsilon)$.

First, the mean meridional mass balance is considered; the total meridional mass transport in each layer is $\overline{v_n h_n}$. Summing over the layers (i.e., vertically integrating) and performing the amplitude expansion, the total mean meridional mass transport is to $O(a^2)$:

$$h^0_1\tilde{v}_1 + h^0_2\tilde{v}_2 + \epsilon\overline{\eta'_1(v'_1 - v'_2)} = 0. \quad (24)$$

The first two terms make up what we term the Eulerian mean (EM) mass transport, which vanishes identically for a geostrophic perturbation (where $v'_1 - v'_2 = \eta'_{1x}$) and is in general nonzero, even for some stable waves. The total mass transport given by (24) leads to the definition of a velocity that is nondivergent and zero for stable waves. This velocity is termed the transformed Eulerian mean (TEM) velocity (Andrews and McIntyre 1976; Shepherd 1983: also referred to as residual mean velocity) and is given by

$$v^*_n \equiv \tilde{v}_n + \frac{\epsilon(\overline{\eta'_n v'_n})}{h^0_n} = \frac{\overline{h_n v_n}}{h^0_n}. \quad (25)$$

The meridional TEM velocity v^*_n is the total meridional mass (heat) transport in a layer, $\overline{h_n v_n}$, divided by the zonal-mean layer depth. As for the EM meridional velocity $\tilde{v}_n$, the TEM meridional velocity v^*_n is $O(\epsilon)$. Substituting into (22)–(23) gives

$$2\omega_I\epsilon v^*_n + \tilde{u}_n + \tilde{\psi}_{ny} = -\epsilon\overline{u'_n v'_{nx}} - \epsilon\overline{v'_n v'_{ny}} + 2\epsilon^2\omega_I\frac{(\overline{\eta'_n v'_n})}{h^0_n} \quad (26)$$

and

$$2\omega_I\epsilon\tilde{\eta}_n + (h^0_n v^*_n)_y = 0. \quad (27)$$

An additional advantage of the TEM formulation is that under *nonacceleration* conditions (Charney and Drazin 1961), when the motion is linear, steady, and adiabatic, the TEM meridional velocity vanishes although the EM may not (Andrews and McIntyre 1976). Thus, the presence of a TEM circulation is evidence of processes that are changing the mean flow.

The zonal mean-flow acceleration (21) can be rewritten as

$$2\omega_I\epsilon\tilde{u}_n = h^0_n(v^*_n q^0_n + \overline{v'_n q'_n}) = \overline{v_n\zeta_{a,n}}. \quad (28)$$

The mean-flow acceleration is driven by the meridional flux of absolute vorticity (ζ_a). Rhines (1977) derived this equation for the QG case, and here it is shown to be true for a shallow-water layered fluid with finite Rossby number as well.

3. Small amplitude mean flow modifications

In this section we compute the mean flow modifications and the meridional mass balance using the theory introduced above. A depth ratio $r = 8$ is chosen so that, at least qualitatively, the result could be applied the results to the Gulf Stream east of Cape Hatteras where the total depth is ~4000 m and the mean thermocline depth is ~500 m. Flows with several different Rossby numbers are considered. For $\epsilon = \sqrt{2}/2$ the jet speed is 1.91 m s^{-1}, similar to that observed in the Gulf Stream (Johns et al. 1995) while the baroclinic transport is 73 Sv (Sv $\equiv 10^6$ m^3 s^{-1}), 40% higher than the observed transport (Hogg 1992). With $g' = 0.0153$ m s^{-2} (Kim and Watts 1994) and $H_1 = 500$ m, the Gulf Stream Rossby number is 0.72. For the SW model with $\epsilon =$

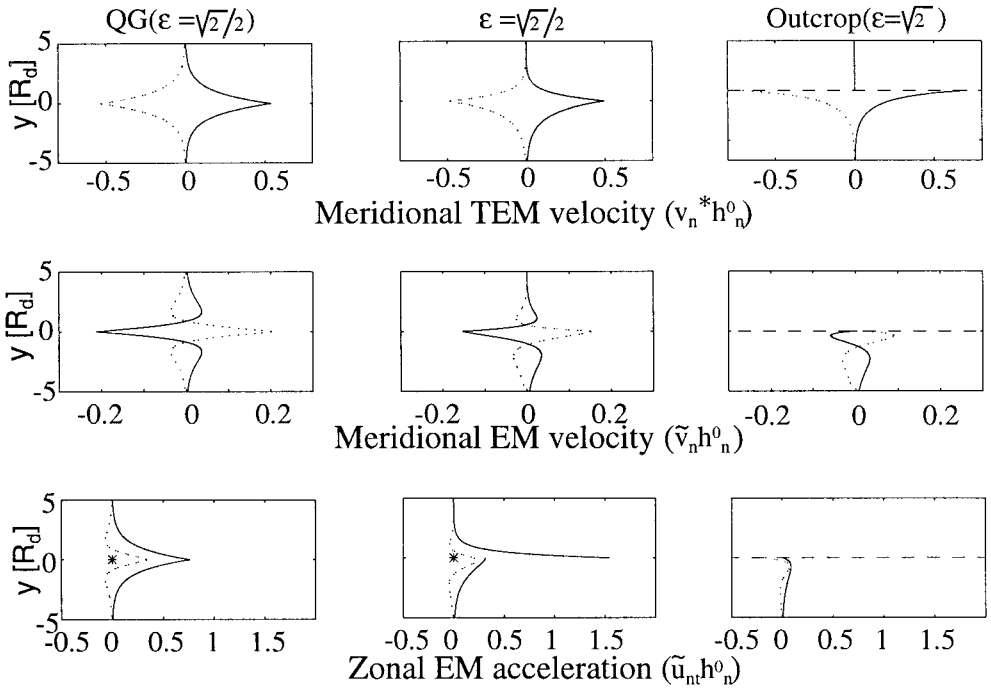

FIG. 2. The transformed Eulerian mean meridional velocity (upper panels), Eulerian mean meridional velocity (middle panels), and mean zonal acceleration (bottom panels) multiplied by the zonal-mean layer thickness ($\overline{h_n} = h_n^0$). Solid line (dotted line) denote the upper (lower) layer. For QG (left panels), $\epsilon = 0.71$ is assumed. All variables are normalized by a^2, where $a = [2 \max(\mu_1(0))]/\lambda$, for each case. An asterisk at the origin denotes a negative δ function of the zonal mean-flow acceleration (see text). A broken line denotes the position of the outcropping front.

$\sqrt{2}/2$, the instability's maximum growth rate is $0.05\epsilon \cdot f \sim 0.27$ day^{-1} (BPT, Fig. 7), slightly higher than 0.22 day^{-1} observed in the Gulf Stream by Watts and Johns (1982). The maximum jet velocity, its transport, and the growth rate all decrease with ϵ and τ (BPT, Fig. 7). The model's mean flow and linear characteristics seem to reproduce those of the Gulf Stream reasonably well.

We define the perturbation amplitude $a \equiv 2\mu_1'(y = 0)/\lambda$, which is the ratio of the maximum horizontal displacement of the front [$\mu_1'(y = 0)$, see (A4)] to the (dimensional) meander wavelength λ. The horizontal displacement of the front (dimensional) will be given by $a\lambda/2$ and since the most unstable wave has length typically $10.5R_d$, $\mu_1'(y = 0) = a \times 5.25R_d$. We normalize all solutions by $O(a^2)$. We also multiply all the computed meridional velocities by the zonal-mean thickness ($\overline{h}_n$) so that we are considering mass transport, and the quantities have a meaningful value at $y = 0$ in the case of the outcropping front (where $\overline{h}_1 = 0$).

In order to find the mean-flow modification, the procedure is to first solve for the TEM velocity and then use that result to find the EM velocity and the mean-flow acceleration. The solution method for finding the TEM velocity is described in appendix A. The mean-flow quantities are computed for three different cases. The first case has $\epsilon = \sqrt{2}/2$, but the QG approximation is assumed (with most unstable wavenumber $k = 0.58$). In the second case, the same ϵ is used, but the SW equations are used ($k = 0.6$), and in the final case, the front outcrops (which implies $\epsilon = \sqrt{2}$, $k = 0.63$). Calculations were also done for values of ϵ in the nonoutcropping SW up to $\epsilon = 1.3$. In all of the mean-flow quantities, the nonoutcropping SW results seem to approach those of the outcropping front as ϵ approaches $\sqrt{2}$. The outcropping case requires special consideration, applying boundary conditions at the outcrop (appendix A).

A cautionary note is warranted here. The outcropping problem can be solved for an infinitesimal perturbation for its linear stability characteristics by arguing that a streamwise coordinate system can be assumed (Killworth et al. 1984; BPT). Some difficulty arises when zonal averaging is applied to regions where only part of the latitude line is covered with fluid (Hayashi and Young 1987). A satisfactory answer to this problem is beyond the scope of this paper, yet it is self-consistent to solve the quasi-linear equations, which apply on the undistorted band of latitudes (Hayashi and Young 1987) using boundary conditions that take the frontal meandering into account (appendix A). It should be kept in mind that the quasi-linear results cannot be compared to numerical results in the areas of a distorted band of latitudes near a finite-amplitude meandering front.

In the upper layer the mean flow is accelerated everywhere except for a δ-function deceleration at the origin ($h_n^0 \tilde{u}_{nt}$, Fig. 2), where the eddy forcing is con-

centrated due to the discontinuity in PV [(28) and (A7)]. In the case of an outcropping front, the singularity disappears since PV in the upper layer is constant. In the lower layer, mean-flow acceleration occurs below the jet and deceleration occurs at the flanks; the maximum in zonal acceleration (multiplied by h_n^0) in the lower layer is slightly south of the front for $\epsilon = \sqrt{2}/2$ and this shift increases with increasing ϵ. This results because in the lower layer, the maximum in the mean PV gradient shifts south as ϵ increases and with it the maximum in perturbation amplitude (BPT, Fig. 6). When the front outcrops, the maximum in zonal acceleration in both layers is well away from the front. The acceleration in both layers is sensitive to the presence of mean flow meridional shear (28) and thus varies significantly in the different flow configurations [see also Shepherd (1987)].

The EM transports ($h_n^0\tilde{v}_n$) are vertically nondivergent for QG (24) and only slightly nondivergent for SW (Fig. 2). In the nonoutcropping cases, the EM circulation consists of three meridional cells similar to the results of Phillips (1954) and Shepherd (1983). In the outcropping case, only two counterrotating cells are present. The lower-layer mean flow modification vanishes north of the front since there are only evanescent tails of the perturbation variables (Killworth et al. 1984) there and $\eta_n' = 0$. The EM meridional transport decreases to zero at the front as ϵ increases and the outcropping case is approached. The maximum in the EM velocity shifts to the south with increasing ϵ in the lower layer but not in the upper layer.

The TEM transport or meridional mass transport is in the direction to reduce potential energy, a signature of baroclinic instability (Fig. 2). It has opposite direction to that of the EM transport in much of the domain. In all cases, $h_n^0 v_n^*$ is maximum at the PV front, $y = 0$ (Fig. 2) where the thickness gradient is the largest. In the upper layer of the outcropping case, the mass flux at the front is performed only by eddies (note that the EM transport is zero there). Under the QG approximation, both the EM and the TEM velocities are $O(\epsilon)$ and we find that in SW, the amplitude of $h_n^0 v_n^*$ is a continuous monotonic function of ϵ (not shown).

The meridional structure of the TEM transport is governed by the baroclinic deformation radius $(1/R_{d,i=1} + 1/R_{d,i=2})^{-1}$, which in QG appears as $(r - 1)/r$ in (A9), the scale of the homogeneous solution. The meridional scale of the eddy fluxes is shorter and contributes to the solution as can be seen in the EM velocity (Fig. 2). The upper-layer zonal acceleration is proportional to the TEM velocity everywhere (28), except at the origin, where $\overline{v_1' q_1'}$ is a δ function in the opposite direction (A7). The north–south asymmetry that appears in the calculation in SW exists because the Rossby radii are different on either side of the front, changing the decay scales of all of the flow variables.

Numerical models results with a small amplitude meander

The changes in the mean flow and the meridional mass transports described in the previous section should only hold for small amplitude meanders as they are derived by performing an amplitude expansion. We check the quasi-linear results against numerical models results with small (but finite) meander amplitudes. We use two different models: a semispectral, doubly periodic rigid-lid QG model as described in Flierl et al. (1987) and a *free surface* isopycnal model developed by Hallberg (1995). We find in most cases that the small amplitude theory does well in predicting the changes to the mean flow. The details of the model runs and their parameters can be found in appendix B.

The QG results compare well with the theoretical ones (compare the left panels of Figs. 2 and 3). The meander amplitude is 0.1 (dimensionally, the displacement of the front is $1.05R_d$). The numerical model results are smoother because there is diffusion in the numerical model. The initial maximum jet velocity is therefore reduced in the upper layer. Differences in circulation intensity are expected due to errors in the amplitude estimation ($\sim \pm 15\%$) and in maximum mean zonal velocity, which was about 30% smaller than U_0. We use (21) and (25) to compute the EM velocities from the acceleration and neglect the dissipation (see appendix B). According to theory, the TEM velocity should be equal and opposite in the two layers, but because dissipation acts differently in the two layers (the velocity shear is larger in the upper layer and thus diffusion is more important there) and because the TEM is a diagnostic quantity in QG, small differences appear. This error also appears in the EM velocities that are not exactly equal and opposite at the front. All variables are symmetric. This symmetry persists as the instability develops and is a strong constraint on the QG dynamics (see below and Nakamura 1993b).

In the SW case of $\epsilon = \sqrt{2}/2$ and a meander amplitude of 0.17 (center panels of Figs. 2 and 3) the TEM is equal and opposite between the layers (a statement that the model conserves mass). The meridional scale of most variables is larger than predicted by the small amplitude theory due to the finite meander amplitude, which in the numerical runs is comparable to the meridional scale in the small amplitude theory. As for QG, the model variables are continuous, smoother than in the theoretical solutions, and agree well in both structure and magnitude (Figs. 2 and 3). Potential errors are due to the perturbation amplitude estimation ($\pm 10\%$) and the reduction of the maximum mean-flow velocity ($\sim 40\%$) from U_0. Unlike QG, the SW, EM, and TEM velocities are slightly asymmetric, consistent with the asymmetry of the mean flow (5)–(6) and the perturbations as found in the linear stability analysis (BPT). There is a small EM velocity in regions where TEM is zero. This feature was absent when we analyzed the same mean flow with

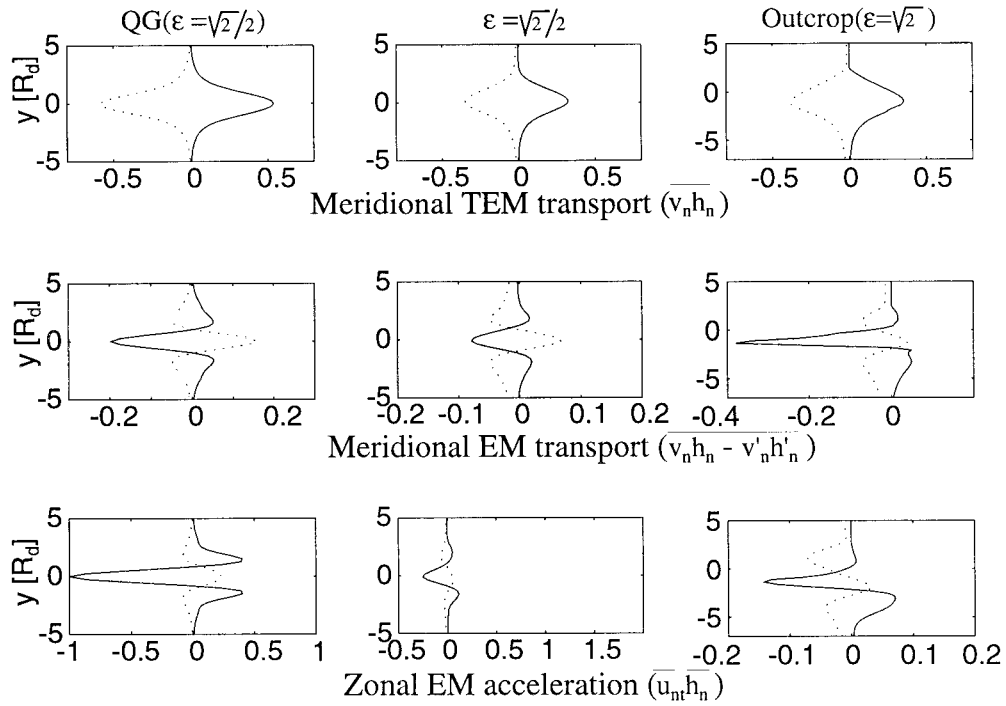

FIG. 3. TEM meridional velocity, EM meridional velocity, and mean-flow acceleration multiplied by the mean layer depth $\overline{h_n}$ for model of PV front ranging from QG (assuming $\epsilon = 0.71$) to a SW outcropping front. Solid (dotted) line denotes upper (lower) layer values. All the variables are normalized by the square of the perturbation amplitude, which for the model ranged from $a \sim 0.1$–0.26 as ϵ varied from QG to the outcropping front (for the meander amplitude in R_d multiply by ~ 5.25). Theoretical predictions for the various cases are displayed in Fig. 2.

a rigid-lid configuration of the isopycnal Miami Community Model (MICOM; Bleck and Boudra 1981), and it is therefore concluded that this result is due to an external (barotropic) mode.

In the previous section it was argued that near the meandering front ($-a < y < a$, $a = 2.73R_d$ for the results of Fig. 3) the quasi-linear solution, derived assuming undistorted latitudes, does not represent well those of the numerical model. Indeed, agreement between the two improves with distance from the front.

In both the zonal acceleration and EM velocity, a strong peak is observed at the southern edge of the outcropping front. In the acceleration, it is reminiscent of the spike observed in the nonoutcropping front due to the singularity in $\overline{v_1' q_1'}$ [(28), bottom panels of Figs. 2 and 3]. The outcropping case in the numerical model has a PV source due to viscous processes damping the mean flow at the meandering front. The zonal velocity has the three cell structure of the nonoutcropping front, the third to the north of the initial frontal position, where the theoretical result is not expected to apply. The mean Eulerian circulations of the outcropping front are very similar to those of the nonoutcropping front (compare center and right panels of Fig. 3), although the southward shifts of the circulation maximum are more apparent in the outcropping case. As in the nonoutcropping case, an external (barotropic) mode with a large meridional scale (the barotropic deformation radius) is observed. This mode does not grow and is overwhelmed by the growing baroclinic mode as the meander amplitude grows.

4. Large amplitude evolution and equilibration

As the meanders grow and equilibrate, the structure of the flow fundamentally changes. The question addressed in this section is whether the insight gained from the quasi-linear theory can help to understand the subsequent evolution of the flow field. We find that the qualitative structure of the mass flux predicted by the quasi-linear theory holds even at finite amplitude and that the seeds of equilibration of the instability can also be found in the quasi-linear theory. Qualitative differences between QG and SW predictions become more pronounced as the meanders grow to large amplitude.

To set the analysis in a context, the energetics of the unstable system is considered. The energetics evolution is very similar among the different flow configurations (Fig. 4). In each case, prior to equilibration, the perturbation energy grows exponentially with a growth rate similar to but slightly less than that predicted by the linear stability calculation for the most unstable wave. The reduction of growth is most likely due to the presence of dissipation in the numerical model (e.g., Pedlosky 1987, his section 7.12). The depth-integrated zonal mean kinetic energy decreases (in the lower layer it

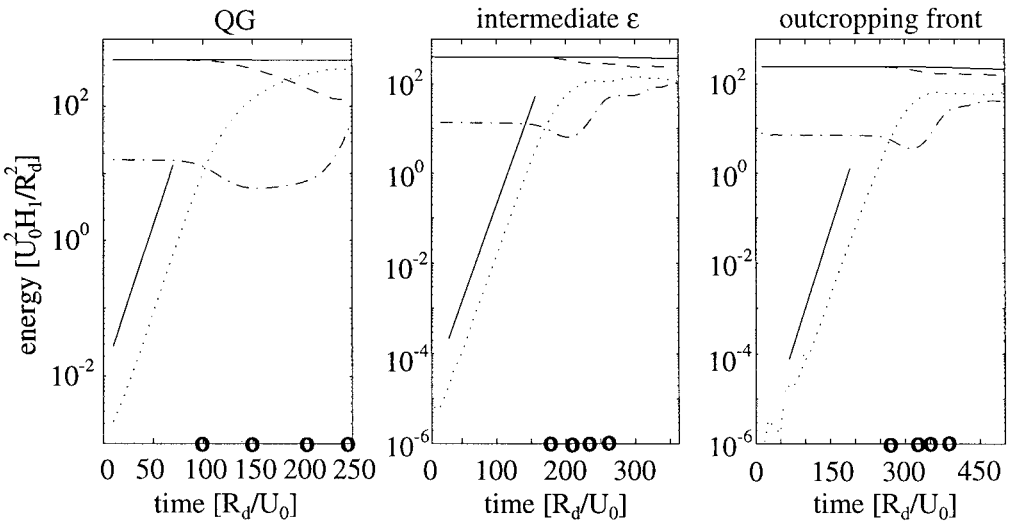

FIG. 4. The evolution of total energy (solid), zonal mean energy (dashed), perturbation energy (dotted), and mean kinetic energy (dot-dashed) as a function of time for models ranging from a QG PV front to the outcropping SW front. The solid line parallel to the perturbation energy curve represents the theoretical growth rate of the instability, $\exp(2\omega_i t)$. Open circles on the x axis denote the times at which the analysis of data was performed. Note the different axes scale for the different model runs.

increases, not shown) even though the y-integrated zonal momentum is conserved because, as predicted from the quasi-linear theory, the upper-layer jet decelerates at the center but accelerates at the flanks (Fig. 3). The perturbation energy increases until equilibration where it is begins to oscillate (Fig. 4), with a superimposed slow (algebraic) growth over a longer timescale (not shown). Note that the perturbation derives its energy from both the kinetic and potential energy of the mean flow and thus the flow may (erroneously) be interpreted as evidence of a mixed (barotropic–baroclinic) instability. The mean flow satisfies only the criteria for baroclinic instability, pointing to the fact that the energetics does not provide sufficient information about the type of instability taking place (Plumb 1983).

QG

As the primary instability equilibrates both the EM and TEM, meridional velocities of the QG case have a similar meridional structure to that of the linear phase of the instability (compare Figs. 3 and 5). The magni-

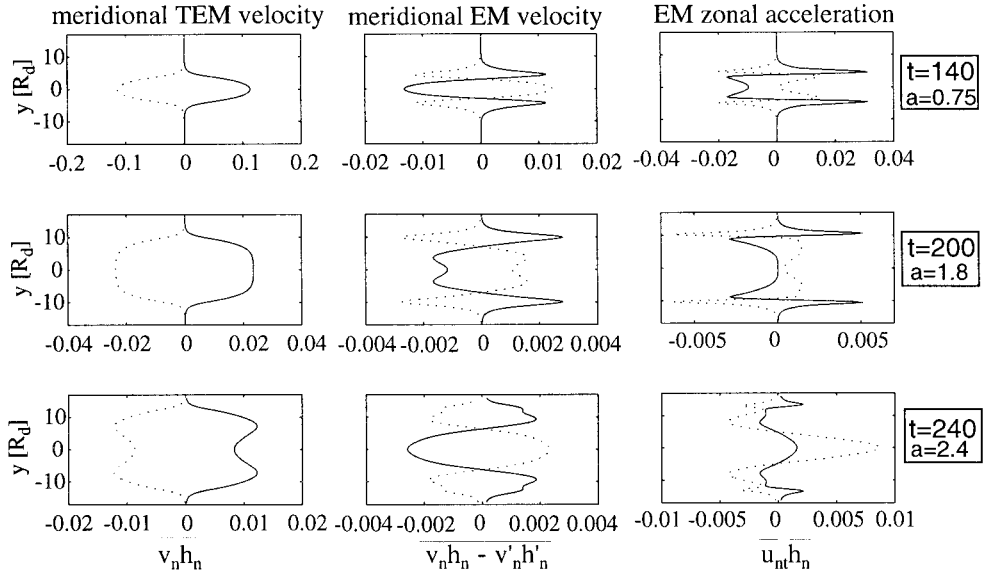

FIG. 5. TEM (left panels), EM (center panels) velocities, and zonal acceleration (right panels) at large amplitude for the QG PV front. Upper (lower) layer values are denoted by solid (dotted) lines. All are normalized by the square of the meander amplitude with a = (0.75, 1.8, 2.4).

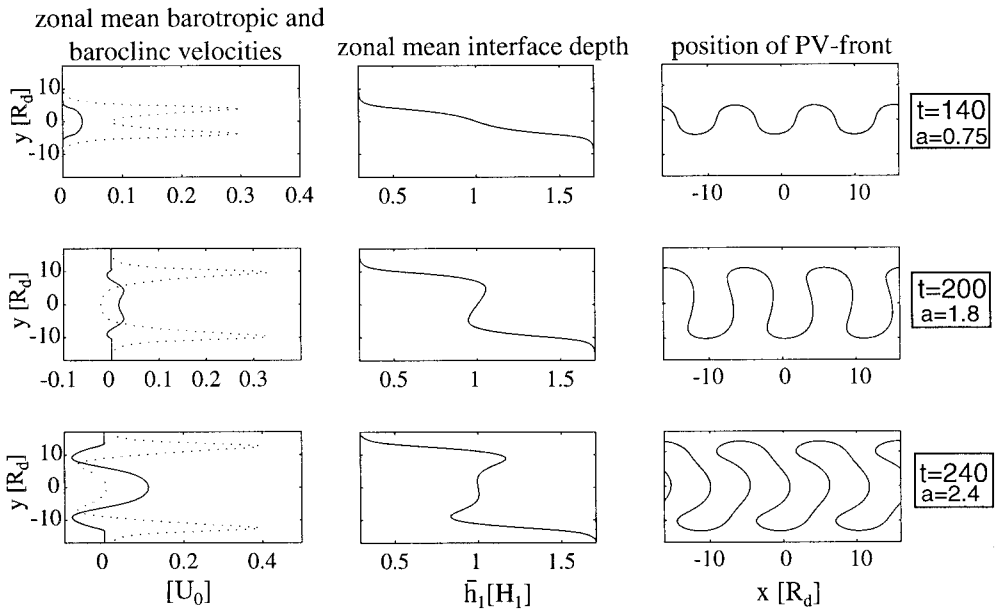

FIG. 6. Barotropic (dotted line) and baroclinic (solid line) mean zonal velocity (left panels, normalized by U_0), upper-layer depth (center panels, normalized by mean upper-layer thickness), and position of the PV front (right panels). The PV front position is represented by the location where $q_1 = q_1(t = 0, y = 0)$.

tudes of both velocities are reduced (when normalized by the perturbation squared; their absolute magnitude actually increases, as long as the perturbation energy does), and their meridional extent increases with the increase in the growth of the meandering front (Fig. 5).

The only dramatic change as a function of time is observed in the mean flow, which becomes barotropic at the center of the jet while becoming strongly baroclinic on the jet's flanks (Fig. 6). This structure is consistent with the quasi-linear theory, which predicts a deceleration of the flow in the upper layer at the front, acceleration on the flanks, and an acceleration at the front in the lower layer. As the instability equilibrates and meander growth is slowed, the northern and southern side of the front are sheared eastward relative to the center.

The presence of barotropic shear was found to reduce the growth rate of baroclinic instability (James 1987; Nakamura 1993b). Together with the reduction in the available potential energy at the flanks, subsequent (secondary) instability growth is expected to be slower than the primary instability. Barotropization of the flow is expected from (28). The equilibration therefore results as from the action of the barotropic shear, accelerated by the growing instability, which causes a reduction in growth and subsequent shearing of the coherent structure of the primary instability. This scenario was termed the barotropic governor by Nakamura (1993a,b).

The QG model equations and initial profile are symmetric about $y = 0$ for all amplitudes (for a proof in a similar case see Nakamura 1993a). This symmetry constraint does not appear in the SW, resulting in a major difference at finite amplitude between the QG and non-QG flows studied here.

1) INTERMEDIATE ϵ

Shallow water mean flow evolution proceeds similarly to that of QG except for the increase in the north–south asymmetry as time increases, especially in the EM meridional transport, although the three-cell structure is maintained. The quasi-linear predictions qualitatively hold and the small-amplitude structure is maintained (compare Figs. 3 and 2 to Fig. 7). The EM meridional velocity becomes more asymmetric with time. Unlike QG, the barotropic flow becomes more antisymmetric after equilibration ($t \sim 225$), which results in strong asymmetries in the shape of the front (Fig. 8). The baroclinic flow remains fairly symmetric as it did in QG.

2) OUTCROPPING FRONT

The evolution and mean-flow structures of the outcropping front evolution are qualitatively similar to the nonoutcropping ones. There is a slight difference in meridional scale (Figs. 9,10). The outcropping front has a cusplike structure (with long tendrils that are formed as the amplitude grows and are mixed into the surrounding fluid). The evolution of the $h_1 = 1$ (500 m) isobath looks very similar to the frontal evolution seen for the asymmetrically evolving nonoutcropping front.

Unlike QG, the location of the PV front is displaced relative to the jet maximum (close to where $h_1 = 1$ in

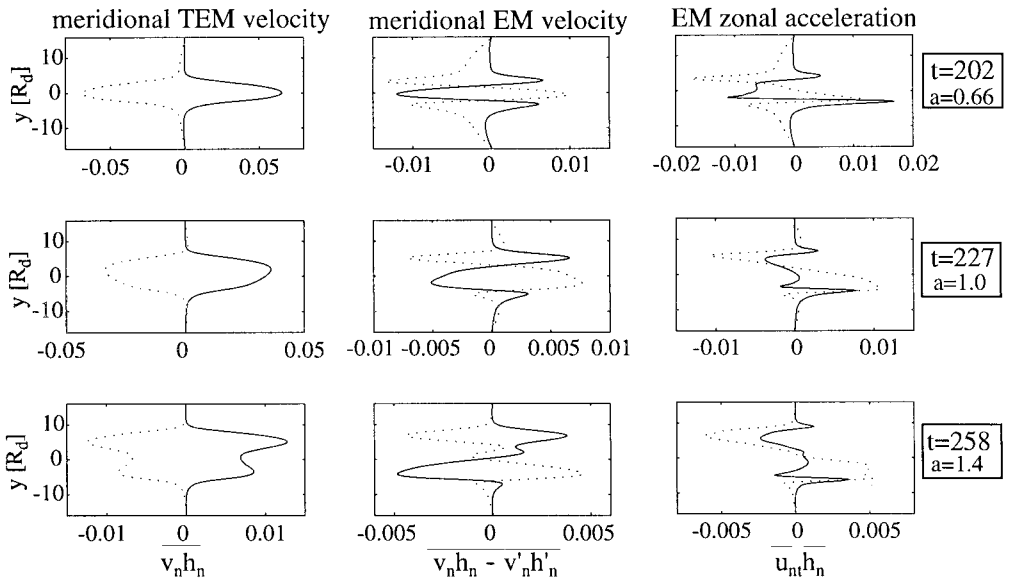

FIG. 7. Same as Fig. 5 but for the SW PV front with $\epsilon = 0.71$.

Fig. 10). This is due to the southward displacement of the maximum in the lower-layer wave amplitude to where there is a PV gradient (BPT, Fig. 6). The separation of the PV front and jet occurs for all $\epsilon > 0$, being most pronounced for the outcropping front. Numerical dissipation of the jet at the outcropping front in the upper layer also contributes to the shift southward of the jet.

5. Discussion and conclusions

In this paper, we formulated and solved the quasi-linear mean-flow modification for small amplitude meanders for a two-layer baroclinically unstable current. We then proceeded to calculate the same quantities in numerical models both at small and finite amplitude. We find the results to be similar for flows ranging from a QG PV front to a SW outcropping front and to hold qualitatively from small to finite amplitude.

The quasigeostrophic approximation misses the asymmetry inherent in SW when the layer depths vary meridionally and the Rossby radius changes. Thus, the fixed stratification assumed in QG causes qualitative errors in the structure of the mean-flow variables. How-

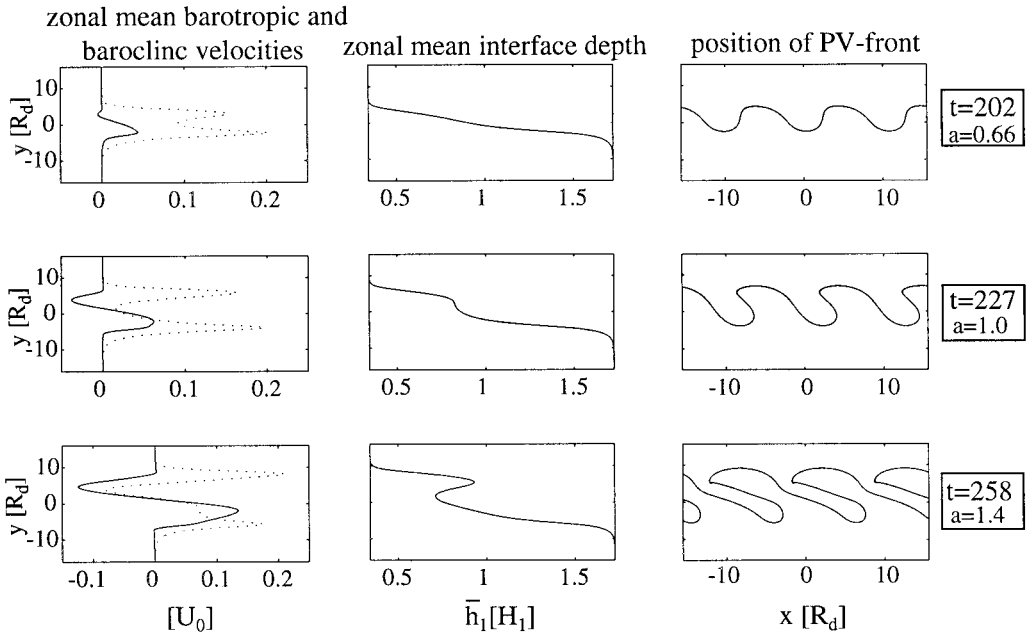

FIG. 8. Same as Fig. 6 but for the SW PV front with $\epsilon = 0.71$.

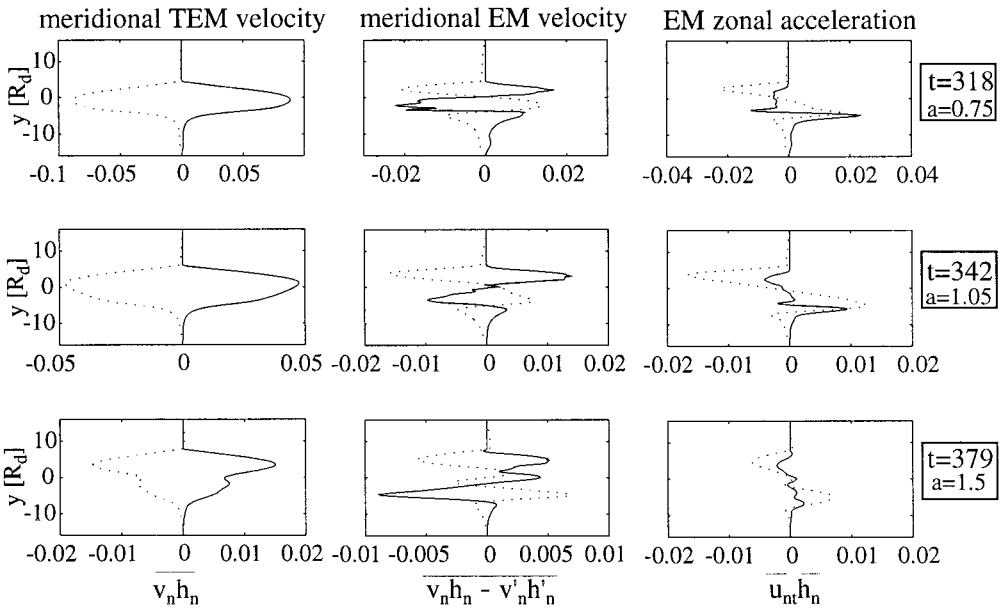

FIG. 9. Same as Fig. 5 but for the outcropping front.

ever, the baroclinic evolution is similar for all models as well as the structure of the mass transport. This similarity also validates the use of R_d as the horizontal scale of the problem for all ϵ [as opposed to, for instance, max(R_{dj})]. This is important when one is interested in using the QG approximation to model geophysical flows with $O(1)$ Rossby numbers.

A second difference between QG and non-QG dynamics is that in finite amplitude the meandering jet is displaced relative to the PV front. This can be traced to the small-amplitude analysis (BPT) where we find the lower-layer perturbation maximum to shift to the south of the PV front, to where the mean PV gradient shifts in the lower layer. As the perturbation grows, the jet's core shifts south relative to the PV front. This shift was found by Wood (1988) in a numerical model analysis of an outcropping front, yet he was not able to explain why it was not found in Ikeda's (1981) QG

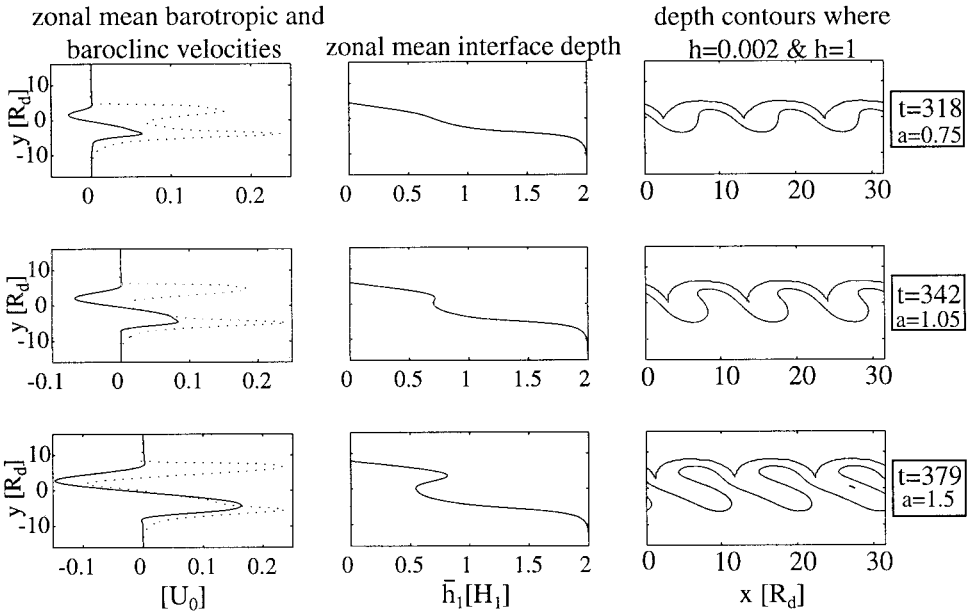

FIG. 10. Same as Fig. 6 but for the outcropping front. Front position is contoured by the position where $h_1 = 0.0002$ (the outcrop), and the $h_1 = 1$ contour is also shown for comparison with Fig. 8.

model. Wood found this shift to be consistent with observations from the Gulf Stream where deep westward recirculation is displaced south relative to the surface jet.

The results of the small-amplitude analysis are found to have predictive value for finite-amplitude perturbations, even beyond the primary instability equilibration. The TEM cell is unidirectional as long as the mean layer interface slope is monotonic with some modification in structure as it reverses sign. Barotropization of the mean flow is predicted by the small-amplitude theory, with the mean barotropic velocity being larger than the mean baroclinic velocity in regions where instability has already taken place. This barotropization has a fundamental role in equilibrating the instability. The small-amplitude theory breaks down in the prediction of the meridional length scale as the meander amplitude grows and the meridional length scale changes from the Rossby radius to the meander amplitude.

The similarities between outcropping and nonoutcropping SW front in the evolution of the $h = 1$ isobath and the structure of the mean variables suggests that the outcrop, while a material barrier, does not influence the qualitative evolution of the instability. This implies that the specific choice of discretization into isopycnal layers for model design is not very important, even when outcropping isopycnals are incorporated. Of course, the number of layers, their angle to the horizontal, and the density differences between the layers are all crucial for the dynamics.

The PV-front model analyzed here does not include planetary PV gradient (the β effect), continuous stratification, topographic slope, and wind-driven convergence, all of which probably have an important influence on Gulf Stream meandering. Another limitation in application of the PV-front model to the Gulf Stream is that the analytical methods used in our study allow only the study of modal waves that are periodic in both the alongfront direction and time [see Boss (1996) for a detailed treatment of these limitations].

Despite its limitations the PV front exhibits several features that are consistent with Gulf Stream observations. First, the basic flow structure captures the PV front observed (Hall and Foffonof 1993) and the baroclinicity of the jet as it leaves the coast. The growth rate of the most-unstable mode is similar to the growth rate of Gulf Stream meanders. Hogg (1992) finds the Gulf Stream alongstream transport relative to 1000 db (a surface-layer transport) to be constant from 73°W near Cape Hatteras to 55°W where Gulf Stream meanders are $O(1)$. Similarly, in the PV-front model, the upper layer has the same transport through the development of the instability, which for the model is a statement of conservation of zonal momentum ($\partial_t \int \overline{h_n u_n}\, dy = 0$).

Watts and coworkers found that QG diagnostics are very useful for interpretation of Gulf Stream data and give similar results to those derived without the QG assumptions (Lindstrom and Watts 1994). This is true in spite of the large Rossby number of the Gulf Stream flow ($\sim$0.7, based on Kim and Watts 1994). Through our analysis, we find that for geostrophic instabilities, QG flows approximate well non-QG flows.

Bower et al. (1985) and Hall and Fofonoff (1993) found the PV front of the Gulf Stream to be displaced to the north (the cyclonic side) of the jet in regions where the jet meanders are $O(1)$. Hall and Fofonoff (1993) PV sections at 68°W and 55°W suggest that this separation increases downstream, where meander amplitude increases. This is consistent with our finding that for a finite Rossby number flow, the two will be displaced and that this displacement increases with the meander amplitude.

The general conclusions of our study have implications for the way the Gulf Stream and similar oceanographic currents have been dynamically interpreted. Quasigeostrophic theory has been used extensively for the dynamical understanding of the Gulf Stream. Our study shows that QG theory does work well for geostrophic instabilities, as long as the appropriate scaling is used. While linear analysis has also been used in the past for the interpretation of Gulf Stream meanders, we use quasi-linear theory to find mean-flow modification from the unstable waves. This allows the study of the causes of the changes in the mean structure of the current as one moves downstream. This analysis of mean-flow modification also allows the explicit linkage of the unstable waves to mean-flow modification and the subsequent increase of the barotropic current and the generation of the Gulf Stream recirculation by eddy potential vorticity fluxes. The evolution of the Gulf Stream as it moves into the extension region can also be interpreted as the equilibration of the Gulf Stream as an unstable flow, and we provide a scenario for understanding how this takes place and, in the process, show that additional effects such as topography are not needed to understand the equilibration.

Acknowledgments. We would like to acknowledge the useful comments of M. Kawase, K. K. Tung, M. Cronin, P. B. Rhines, and D. Swift. D. Darr assisted with the SW numerical model runs. Numerical models were kindly provided by G. Flierl, R. Hallberg, and E. Chassignet. Comments of an anonymous reviewer have greatly improved the manuscript and made us realize the limitation with the quasi-linear analysis of the outcropping front. E.B. is supported by a National Science Foundation Young Investigator Award to L.T., and L.T. by an Office of Naval Research Young Investigator Award.

APPENDIX A

Method of Solution of the Mean-Flow Quasi-Linear Equations

In order to solve for the TEM meridional velocity we combine (21), (26), and (27) to get an equation for $V_1^* \equiv \overline{h}_1 v_1^* = \overline{h}_1 v_1$,

$$V^*_{1yy} - V^*_1\left[q^0_1 + q^0_2 + 4\omega_I^2\epsilon^2\left(\frac{1}{h^0_1} + \frac{1}{h^0_2}\right)\right]$$
$$= h^0_1\overline{v'_1q'_1} - h^0_2\overline{v'_2q'_2}\,2\omega_I\epsilon^2(\overline{u'_1v'_{1x}} + \overline{v'_1v'_{1y}} - \overline{u'_2v'_{2x}} + \overline{v'_2v'_{2y}}) - 4\omega_I^2\epsilon^3\left(\frac{(\overline{\eta'_1v'_1})}{h^0_1} - \frac{(\overline{\eta'_2v'_2})}{h^0_2}\right), \quad \text{(A1)}$$

where we have substituted $2\omega_I$ for ∂_t.

Equation (A1) is a second-order ODE, whose rhs we know from the $O(a)$ solutions. The growth rate (ω_I) is small [$O(0.1)$] for all ϵ and therefore the same terms that dominate in QG dominate in the SW solution.

The boundary conditions (BCs) and matching conditions for the nonoutcropping front are

$$V^*_1(y = \pm\infty) = 0 \quad \text{and}$$
$$[dV^*_1/dy]^+_- = \lim_{b\to 0}\int_{-b}^{b} h^0_1\overline{q'_1v'_1}\,dy, \quad \text{(A2)}$$

where $[\theta]^+_- \equiv \theta(0^+) - \theta(0^-)$. The BC is that the solution is trapped to the front (as are the perturbations), while the matching condition is derived from (A1) requiring that V^*_1, the mass flux, be continuous at $y = 0$.

For the outcropping case there is an additional boundary condition at the outcrop, $y = 0$. There $\tilde{v}_1(0)$ is finite while $h^0_1(0) = 0$ in (25) so that

$$V^*_1(y = 0^-) = \epsilon\overline{\eta'_1v'_1(y = 0)}.$$

The PV flux composes part of the forcing terms on the rhs of (A1) and can be found as follows. The PV is governed by $Dq_n/Dt = 0$. The $O(a)$ PV evolution equation is (after division by $e^{i(kx-\omega t)}$)

$$D_nq'_n = ik(u^0_n - c)q'_n = -v'_nq^0_{ny}, \quad \text{(A3)}$$

which can be combined into

$$D_n(q'_n + \mu'_nq^0_{ny}) = 0, \quad \text{(A4)}$$

where the meridional displacement is found from $D\mu'_1/Dt = ik(u^0_1 - c)\mu'_1 = v'_1$. If we assume no initial perturbation in the PV (Rhines and Holland 1979), then

$$q'_n = -\mu'_nq^0_{ny}. \quad \text{(A5)}$$

For the PV-front model

$$q^0_{1y} = \delta(y)(q_{12} - q_{11}) \quad \text{(A6)}$$

so that

$$\overline{v'_1q'_1} = -q^0_{1y}\overline{v'_1\mu'_1} = \delta(y)(q_{11} - q_{12})\overline{v'_1\mu'_1}. \quad \text{(A7)}$$

Here $\delta(y)$ denotes a δ function centered at $y = 0$. Thus, the matching condition in (30) becomes

$$[dV^*_1/dy]^+_- = (q_{11} - q_{12})h^0_1(0)\overline{v'_1(0)\mu'_1(0)}. \quad \text{(A8)}$$

For a QG flow the TEM equation (A1) simplifies to

$$V^*_{1yy} - V^*_1\left(\frac{r}{r-1}\right) = \epsilon\overline{v'_1u'_{1y}} + \epsilon\overline{v'_2u'_{2y}} - \epsilon(\overline{\eta'_1v'_1}) + \frac{\epsilon(\overline{\eta'_2v'_2})}{r-1} = h^0_1\overline{v'_1q'_1} - h^0_2\overline{v'_2q'_2}. \quad \text{(A9)}$$

Equation (A9) can be solved analytically, once the rhs is evaluated from the $O(a)$ solution. Substituting (A7), (A9) becomes

$$V^*_{1yy} - V^*_1\left(\frac{r}{r-1}\right) = \delta(y)(q_{11} - q_{12})\overline{v'_1\mu'_1} - (r-1)\overline{v'_2q'_2}. \quad \text{(A10)}$$

Using the Green's function technique (e.g., Bender and Orzag 1978, 16–19),

$$V^*_1(y) = \frac{(r-1)\gamma}{2}\int_{-\infty}^{\infty} e^{-|y-\alpha|/\gamma}\overline{v'_2q'_2}(\alpha)\,d\alpha + \frac{\gamma e^{-|y|/\gamma}}{2}(q_{12} - q_{11})\overline{v'_1(0)\mu'_1(0)}, \quad \text{(A11)}$$

where the Green's function is $-\gamma e^{-|y-\alpha|/\gamma}/2$ and $\gamma \equiv \sqrt{(r-1)/r}$. $\overline{u}_1(0) = 1$ and $q_{12} - q_{11} = 2\epsilon + O(\epsilon^2)$ (BPT) so that

$$V^*_1(y) = \frac{(r-1)\gamma}{2}\int_{-\infty}^{\infty} e^{-|y-\alpha|/\gamma}\overline{v'_2q'_2}(\alpha)\,d\alpha + \epsilon\gamma e^{-|y|/\gamma}\overline{v'_1(0)\mu'_1(0)}. \quad \text{(A12)}$$

We solve (A1) for finite ϵ using a relaxation technique with the forcing given from the $O(a)$ solution. Since the domain is infinite, we first map to a finite domain, using the monotonicity of $U = u^0_1$ in each of the half-infinite domains. Then (A1) is

$$\alpha_j^2U^2V^*_{1UU} + \alpha_j^2UV^*_{1U} - G(U)V^*_1 = F(U), \quad \text{(A13)}$$

where $\partial_y = \pm\alpha_jU\partial_U$ and with

$$G(U) = \alpha_j^2 + \frac{1}{h^0_2} + 4\omega_I^2\epsilon^2\left(\frac{1}{h^0_1} + \frac{1}{h^0_2}\right),$$
$$F(U) = h^0_1\overline{v'_1q'_1} - h^0_2\overline{v'_2q'_2} + -2\omega_I\epsilon^2(\overline{u'_2v'_{2x}} - \overline{u'_1v'_{1x}} - \overline{v'_1v'_{1y}} + \overline{v'_2v'_{2y}}) - 4\omega_I^2\epsilon^3\left(\frac{(\overline{\eta'v'_1})}{h^0_1} + \frac{(\overline{\eta'v'_2})}{h^0_2}\right).$$

The boundary conditions are $V^*_1(y = \pm\infty) = 0$ and (A2). The domain is discretized using $O(100–1000)$ grid intervals of equal ΔU. Writing the derivatives in their finite difference form [we used second-order accurate $O(\Delta U)^2$, e.g., Abramowitz and Stegun 1965], (A13) is written as a matrix equation with the jump condition in dV^*_1/dy used to patch the two half domains. In the out-

cropping case the solution is calculated only in the south side.

We tested our relaxation scheme by making sure the QG solution is retrieved when $\epsilon \to 0$ and by making sure that zonal momentum is conserved.

APPENDIX B

Numerical Models Used and Their Parameters

We use two different numerical models: a semispectral, doubly periodic rigid-lid QG model as described in Flierl et al. (1987) and a *free surface* isopycnal model developed by Hallberg (1995). The QG model has Laplacian dissipation, while the isopycnal model uses biharmonic diffusion. Quantitative comparisons with a *rigid-lid* version of the Miami community model (courtesy of E. Chassignet) find good agreement for cases with no outcropping layers. Unfortunately the rigid-lid model was unsuccessful in the outcropping front case because of a problem in the boundary conditions of the Poisson solver for the barotropic mode (E. Chassignet 1996, personal communication). We therefore use a free-surface model, even though it has additional dynamics not encompassed by our analytical model, namely those of barotropic waves.

All of the model runs are initialized with (5)–(6) as the initial mean-flow profile with no flow in the lower layer. The flow domain is chosen to be square with a length three times the most unstable wavelength, as calculated from theory (BPT). In order to accelerate the growth of the most unstable normal mode, the flow in the upper layer is initialized with a small-amplitude periodic perturbation ($a = [2\mu_1'(y = 0)]/\lambda \sim 0.001$–$0.01$) that has some energy in the most unstable mode. The perturbation has some PV signature (unlike the pure normal mode), but it is much smaller then the background PV. Since the energy of the initial perturbation is not only in the most unstable wave, the growth rate of the perturbation energy does not initially increase exponentially, nor can we observe the most unstable mode (against its background) until its amplitude reaches $O(0.05)$. One could not use a much smaller initial perturbation because numerical dissipation would strongly affect the mean flow before the perturbation grows to $O(1)$. The model runs analyzed are included in Table B1. We performed many more runs, varying dissipation, grid size, number of grid points (and thus number of wavelengths in the domain), and time steps, and did not find notable differences with the results presented here.

We calculate the perturbation amplitude (a) as the distance between the southern and northern maximum (D) in zonal velocity divided by 2 and normalized by half the meander wavelength, $a = 2D/\lambda \pm 2\Delta y/\lambda$. The error in the estimation of a is due to the finite size of grid boxes, and we used contour plots of the PV front to refine the estimate of a at small amplitude. Until the primary instability equilibrates, the amplitude is observed to grow like $e^{\omega_i t}$. The meander propagation speed (c_r) also agrees well with linear instability calculation (not shown).

TABLE B1. The different runs analyzed here: RE $= U_0 R_d/\kappa$ for QG and $R = U_0 R_d^3/\nu$ for the isopycnal SW model where κ is the numerical Fickian diffusion coefficient (QG) and ν the biharmonic diffusion coefficient (SW). All the variables are nondimensionalized by U_0 and R_d.

Model	Profile	$\Delta x = \Delta y$	Δt	Re or R
QG	QG	0.254	0.05	10^4
SW	$\epsilon = \frac{\sqrt{2}}{2}$	0.247	0.015	5800
SW	$\epsilon = \sqrt{2}$	0.235	0.03	795

In the QG approximation we cannot estimate the EM and TEM velocities directly from the numerical output since they are $O(\epsilon)$ quantities. They are calculated diagnostically using the mean-flow acceleration equation (28), which with a viscous term added is

$$\epsilon\overline{u}_{nt} - \overline{h}_n(\overline{q}_n v_n^* + \overline{v_n' q_n'}) = \epsilon\overline{u}_{nt} - \overline{h_n q_n v_n} = \frac{1}{\mathrm{Re}}\overline{u}_{nyy}, \tag{B1}$$

where $\mathrm{Re} = \nu/(U_0 R_d)$ is the Reynolds number and ν the numerical Laplacian viscosity. Since $\mathrm{Re} = 10^4$ for the QG run presented here, the diffusive term is neglected and we use (21) and (25) to calculate v_n^* and $\tilde{v}_n$: $\tilde{u}_{nt}$ and the zonally averaged eddy correlations are calculated directly from the numerical simulation (e.g., $\overline{u_{nt}}$). The error is expected to be largest at the front in the upper layer where the rhs of (42) is maximum.

In the shallow water case the mean zonal accelerations $\overline{h_n}\,\overline{u_{nt}}$ and the mean meridional mass fluxes $\overline{h_n v_n}$ were calculated directly by zonally averaging the model output. The EM velocity was calculated from (25).

All the results are nondimensionalized by U_0 the initial maximum jet velocity H_1, the initial *meridional* mean upper-layer depth, and the Rossby radius based on it, $R_d = \sqrt{g' H_1}/f$.

The model energetics are calculated using the standard method of dividing each variable to a zonal mean ($\overline{\theta}$) and a perturbation from it ($\theta' = \theta - \overline{\theta}$). We then calculate the mean zonal kinetic and potential energy (calculated using $\overline{\theta}$) and the perturbation energy that results from correlation between perturbation quantities.

REFERENCES

Abramowitz, M., and I. A. Stegun, 1965: *Handbook of Mathematical Functions.* Dover, 1046 pp.

Andrews, D. G., and M. E. McIntyre, 1976: Planetary waves in horizontal and vertical shear: The generalized Eliassen–Palm relation and the mean zonal acceleration. *J. Atmos. Sci.*, **33,** 2031–2048.

Bender, C. M., and S. A. Orzag, 1978: *Advanced Mathematical Methods for Scientists and Engineers.* McGraw-Hill.

Bleck, R., and D. B. Boudra, 1981: Initial testing of a numerical ocean circulation model using a hybrid (quasi-isopycnic) vertical coordinate. *J. Phys. Oceanogr.,* **11,** 755–770.

Boss, E., 1996: Dynamics of potential vorticity fronts. Ph.D. thesis, University of Washington, 168 pp.

——, N. Paldor, and L. Thompson, 1996: Stability of a potential vorticity front: From quasi-geostrophy to shallow water. *J. Fluid Mech.,* **315,** 65–84.

Bower, A. S., H. T. Rossby, and J. L. Lillibridge, 1985: The Gulf Stream—Barrier or blender? *J. Phys. Oceanogr.,* **15,** 24–32.

Charney, J. G., and P. G. Drazin, 1961: Propagation of planetary-scale disturbances from the lower into the upper atmosphere. *J. Geophys. Res.,* **66,** 83–109.

Flierl, G. R., and A. R. Robinson, 1984: On the time dependent meandering of a thin jet. *J. Phys. Oceanogr.,* **14,** 412–423.

——, P. Malanotte-Rizzoli, and N. J. Zabusky, 1987: Nonlinear waves and coherent vortex structures in barotropic β-plane jets. *J. Phys. Oceanogr.,* **17,** 1408–1438.

Hall, M. M., and N. P. Fofonoff, 1993: Downstream development of the Gulf Stream from 68° to 55°W. *J. Phys. Oceanogr.,* **23,** 225–249.

Hallberg, R., 1995: Some aspects of the circulation in ocean basins with isopycnals intersecting sloping boundaries. Ph.D. thesis, University of Washington, 244 pp.

Hayashi, Y. Y., and W. R. Young, 1987: Stable and unstable shear modes of rotating parallel flows in shallow water. *J. Fluid Mech.,* **184,** 477–504.

Hogg, N. G., 1992: On the transport of the Gulf Stream between Cape Hatteras and the Grand Banks. *Deep-Sea Res.,* **39,** 1231–1246.

Ikeda, M., 1981: Meanders and detached eddies of a strong eastward-flowing jet using a two-layer quasi-geostrophic model. *J. Phys. Oceanogr.,* **11,** 526–540.

James, I. N., 1987: Superposition of baroclinic instability in horizontally sheared flows. *J. Atmos. Sci.,* **44,** 3710–3720.

Johns, W. E., T. J. Shay, J. M. Bane, and D. R. Watts, 1995: Gulf Stream structure, transport and recirculation near 68°W. *J. Geophys. Res.,* **100,** 817–838.

Killworth, P. D., N. Paldor, and M. E. Stern, 1984: Wave propagation and growth on a surface front in a two-layer geostrophic current. *J. Mar. Res.,* **42,** 761–785.

Kim, H.-S., and D. R. Watts, 1994: An observational streamfunction in the Gulf Stream. *J. Phys. Oceanogr.,* **24,** 2639–2657.

Lindstrom, S. S., and D. R. Watts, 1994: Vertical motion in the Gulf Stream near 68°W. *J. Phys. Oceanogr.,* **24,** 2321–2333.

Nakamura, N., 1993a: An illustrative model of instabilities in meridionally and vertically sheared flows. *J. Atmos. Sci.,* **50,** 357–375.

——, 1993b: Momentum flux, flow symmetry, and the nonlinear barotropic governor. *J. Atmos. Sci.,* **50,** 2159–2179.

Onken, R., 1992: Mesoscale upwelling and density finestructure in the seasonal thermocline—A dynamical model. *J. Phys. Oceanogr.,* **22,** 1257–1273.

Paldor, N., 1983: Linear stability and stable modes of geostrophic fronts. *Geophys. Astrophys. Fluid Dyn.,* **24,** 299–326.

Pedlosky, J., 1970: Finite-amplitude baroclinic waves. *J. Atmos. Sci.,* **27,** 15–30.

——, 1987: *Geophysical Fluid Dynamics.* Springer-Verlag, 710 pp.

Phillips, N. A., 1954: Energy transformations and meridional circulations associated with simple baroclinic waves in a two-level, quasi-geostrophic model. *Tellus,* **6,** 273–286.

Plumb, R. A., 1983: A new look at the energy cycle. *J. Atmos. Sci.,* **40,** 1669–1688.

Pratt, L. J., and M. E. Stern, 1986: Dynamics of potential vorticity fronts and eddy detachment. *J. Phys. Oceanogr.,* **16,** 1101–1120.

Rhines, P. B., 1977: The dynamics of unsteady currents. *The Sea,* Vol. 6, E. D. Goldberg, Ed., John Wiley and Sons, 189–318.

——, and W. R. Holland, 1979: A Theoretical discussion of eddy-driven mean flows. *Dyn. Atmos. Oceans.,* **3,** 289–325.

Shay, T. J., J. M. Bane, D. R. Watts, and K. L. Tracey, 1995: Gulf Stream flow field and events near 68°W. *J. Geophys. Res.,* **100,** 22 565–22 589.

Shepherd, T. G., 1983: Mean motions induced by baroclinic instability in a jet. *Geophys. Astrophys. Fluid Dyn.,* **27,** 35–72.

Stommel, H., 1965: *The Gulf Stream.* University of California Press, 248 pp.

Watts, D. R., and W. E. Jones, 1982: Gulf Stream meanders; observations on propagation and growth. *J. Geophys. Res.,* **87,** 9467–9476.

——, K. L. Tracey, J. M. Bane, and T. J. Shay, 1995: Gulf Stream path and thermocline structure near 74°W and 68°W. *J. Geophys. Res.,* **100,** 18 291–18 312.

Williams, R., 1991: Primitive equation models of Gulf stream meanders. WHOI Tech. Rep. WHOI-92-16, 272–285.

Wood, R. A., 1988: Unstable waves on oceanic fronts: Large amplitude behavior and mean flow generation. *J. Phys. Oceanogr.,* **18,** 775–787.